22nd International Symposium on Plasma Chemistry
July 5-10, 2015; Antwerp, Belgium

Development of a DFT-based KMC model for Ni-catalyzed plasma dry reforming

M. Shirazi, E.C. Neyts and A. Bogaerts

Research Group PLASMANT, Department of Chemistry, University of Antwerp, 2610 Antwerpen-Wilrijk, Belgium

Abstract: In this contribution, we use density functional theory (DFT) calculations to investigate the interaction of radicals and molecules, formed in a CO_2/CH_4 plasma, with a (catalytic) Ni(111) surface. The possible reaction pathways for the desired products are identified, which is of great interest for plasma catalysis. The dependence of the reaction kinetics on the local chemistry is translated into a 3D lattice-based kinetic Monte Carlo (KMC) model. The DFT+KMC model provides a distinct method to investigate the competition between various reaction pathways. By modifying the partial pressure of the plasma species, we can investigate how desired products can be selectively produced from the catalyst surface.

Keywords: plasma catalysis, DFT, KMC

1. Introduction

Global warming is a consequence of a rise in the concentration of greenhouse gases in the earth's atmosphere. This rise started since the beginning of the industrial revolution, which resulted in an increase in the global air and sea surface temperature. The two most abundant gases are carbon dioxide (CO_2) and methane (CH_4). The atmospheric concentration of carbon dioxide continues to increase by burning of fossil fuels and clearing of native forests. Also the methane concentration has been rising as a consequence of human activities such as leakage from natural gas systems and the raising of livestock.

Dry reforming of methane is a solution to convert both greenhouses gases into syngas, which is desirable for many industrial synthesis processes:

$$CO_2 + CH_4 \rightarrow 2\,H_2 + 2\,CO \quad \Delta H^\circ = 247 \text{ kJ/mol} \quad (1)$$

Both CO_2 and CH_4 molecules are chemically inert and thermodynamically stable. In conventional methods, the conversion of these gases into a valuable feedstock occurs in the presence of a metal-based catalyst at high temperature and pressure (catalyst-based dry reforming), but it can also take place in the presence of plasma at low temperature and atmospheric pressure (plasma-based dry reforming). Both methods face difficulties. Catalyst-based dry reforming is subject to coke deposition and a slow start-up time. Plasma-based dry reforming shows a lack of selectivity [1-2].

Recently, it has been shown that there is a synergy between plasma and catalysis processes. The synergic interaction between reactive species in the plasma environment and at the catalyst surface accelerates the catalytic reactions. However, there are still many unknown physical and chemical reactions in a plasma-catalysis process [3].

In this study, we attempt to unravel the interaction of radicals and molecules with a bulk-terminated Ni(111) catalyst surface. The chemical reactions are investigated at the atomic scale using density functional theory (DFT) [4]. This includes the reaction energies and reaction kinetics of possible chemical reactions. The possible reaction pathways are identified and activation energies for the formation of added-value chemicals are calculated. Secondly, the established chemical reactions are implemented into a kinetic Monte-Carlo (KMC) model. The role of each chemical reaction and its consequence on other chemical reactions at an extended time and a larger scale is investigated.

The combined model (DFT+KMC) will allow us to explain the efficiency and selectivity of the underlying mechanisms of plasma-catalysis.

2. Computational details

2.1. Density functional theory

To model the interaction of radicals with a Ni catalyst, self-consistent DFT in the GGA approximation [4] was employed. The reaction energies, activation energies and ab initio molecular dynamics (MD) of the system were calculated in a 3D periodic model, utilizing VASP [5]. In these calculations, the electronic energies were approximated using the PAW description of atomic cores and the functional of PBE. The plane wave cut off energy was 400 eV. For Ni atoms $3d^8 4s^2$, O atoms $2s^2 2p^4$, and C atoms $2s^2 2p^2$ electrons were included as valence electrons. All calculation of radicals were open shell. The self-consistent steps were converged to an energy difference of 10^{-4} eV.

Geometries were optimized using the conjugate-gradient scheme with no symmetry restraints and no fixed atoms to a convergence of gradients of less than 10^{-3} eV/Å.

Converged values of the surface energies of the (111)

surfaces showed that three layers of Ni are enough to be considered as the slab. To avoid slab-slab interaction in the periodic model, 10 Å was regarded as the vacuum distance. The k-point sampling in reciprocal space was generated by the Monkhorst-Pack method. 4×4×4 and 4×4×1 grid sizes were utilized for bulk and slab, respectively. For the surface, we used a three-layered 2×2 supercell and the k-point sampling was reduced to 2×2×1.

2.2. Kinetic Monte-Carlo

In order to track the surface evolution, a lattice based KMC method is used. The lattice can in principle be two or three dimensional. Three dimensional sites are chosen to accurately translate the topological complexity of chemical reactions from the atomistic simulation to the KMC simulation. The lattice sites are defined based on two layers of a Ni (111) surface. The three-dimensional lattice surface sites are Ni sites, hcp sites and fcc sites. Initially, the Ni sites are occupied by Ni atoms, while the hcp and fcc sites are empty sites. In the Ni (111) structure, every Ni site is surrounded by three fcc sites and three hcp sites. Based on the counted number of first neighbours of a site, the coordination number (c.n.) is defined. Every Ni site can have a c.n. ranging from 9 up to 15 and every hcp or fcc site can have a c.n. ranging from 0 to 3.

Each lattice site is associated with three variables describing the state of this site:

- The first variable contains the information regarding the chemical identity of the site. This variable is updated frequently during the KMC simulation.
- Each lattice site also has a neighbour list that carries the information about the local bonding. Local bonding indicates which site is connected to which site and this assists in defining the reaction events in KMC.
- Finally, each lattice site is associated with a discrete variable describing the c.n. of the site. This variable, together with the neighbour list, allows us to implement the complicated chemistry at the surface.

In our KMC model, reaction events are defined and used to implement the chemistry of plasma catalysis obtained from the DFT calculations. For every position, geometry optimization was carried out by DFT calculations. The minima obtained from the DFT calculations are mapped onto the lattice sites for the subsequent KMC calculations. The events taking place in the KMC calculation modify the chemical occupation of the sites. This corresponds to the transition of the system from one minimum to another in the DFT calculation. The frequency of occurrence of an event is derived using the Eyring equation, with the activation energy obtained from NEB calculations [6] implemented in VASP.

The so-called plasmaK application was developed as a new feature in the stochastic parallel particle kinetic simulator (SPPARKS) code [7-8].

3. Results and discussion

3.1. DFT results

In this section, we only describe the formation of the added-value chemicals. This includes methanol (CH_3OH), formaldehyde (CH_2O), C1-C2 hydrocarbons and formic acid (HCOOH). All the other reactions, such as adsorption of free radicals, surface reconstruction, Eley-Rideal mechanisms, and deactivation of the catalyst surface, are not included in this abstract, because of limited space.

3.1.1. Methanol

Three different reaction pathways result in the formation of methanol.

First, an O atom is introduced to the adsorbate CH_3. The adsorption of the O atom gives rise to the formation of a CH_2OH adsorbate. The NEB calculations show that the desorption of radicals or charged species is highly endothermic. Hence, the protonation of CH_2OH is the most probable chemical reaction. Fig. 1a shows a CH_2O fragment adsorbed on the Ni surface. Fig. 1b shows the transition state geometry for protonation of CH_2OH. This protonation leads to the formation and desorption of CH_3OH, as shown in Fig. 1c.

The associated activation energy was calculated for different H coverages (Table 1: reactions 1 and 2). The rate of proton diffusion increases due to the increase of the proton coverage and this reaction becomes more exothermic.

Table 1. Protonation of various adsorbate species, yielding the formation of methanol, for different proton coverages.

	Reaction	Coverage (H/nm^2)	E_a (eV)	ΔE
1.	$CH_2OH(s)+H(s)\rightarrow CH_3OH(g)$	8	0.49	-0.18
2.	$CH_2OH(s)+H(s)\rightarrow CH_3OH(g)$	16	0.37	-0.34
3.	$OCH_3(s)+H(s)\rightarrow CH_3OH(g)$	20	0.31	-1.04
4.	$OCH_3(s)+H(s)\rightarrow CH_3OH(g)$	20	0.25	-0.98
5.	$CO_2CH_3(s)+H(s)\rightarrow CH_3OH(g)+CO(s)$	12	1.20	-1.33
6.	$CO_2CH_3(s)+H(s)\rightarrow CH_3OH(g)+CO(s)$	16	0.44	-0.37
7.	$CO_2CH_3(s)+H(s)\rightarrow CH_3OH(g)+CO(s)$	20	1.31	-1.14

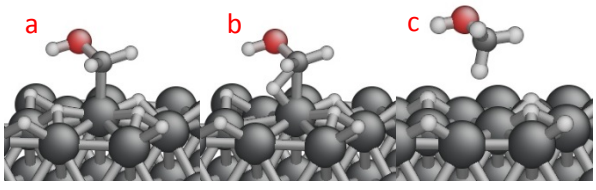

Fig. 1. Protonation of CH_2OH to methanol; a) shows the formation of CH_2OH; b) shows the saddle point; and c) shows the formation and desorption of methanol.

In the second pathway, CH_3 is introduced to an adsorbed O atom. This causes the formation of CH_3O;

see Fig. 2a. The activation energies and reaction energetics of CH_3OH formation are also indicated in Table 1 (reactions 3 and 4). This time, a different proton from the surface is considered. This makes the activation energy different for the same coverage since the position of the proton is different. Both activation energies are below 0.4 eV. Furthermore, this reaction is exothermic and causes the formation and desorption of CH_3OH; see Fig. 2b. Hence, we did not consider higher proton coverages.

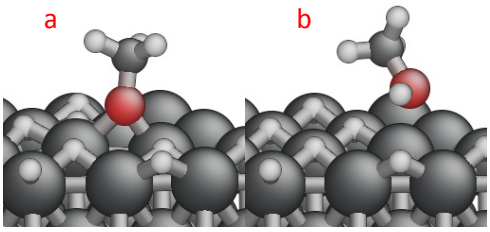

Fig. 2. Protonation of CH_3O to methanol; a) shows the formation of CH_3O; and b) shows the protonation and desorption of methanol.

In the third pathway, CH_3 is introduced to adsorbed CO_2; see Fig. 3a. Proton diffusion to the oxygen of CO_2-CH_3 will lead to the formation of CH_3OH and CO; see Fig. 3b. Diffusion of a proton to oxygen will cause bond breaking between C-O and adsorption of CO at the surface: see Fig. 3b. In contrast to the above reactions, the increase of the proton coverage does not lead to a reduction of the activation energy (Table 1, reactions 5 to 7). The activation energy is reduced from 1.20 eV for 12 H/nm^2 to 0.44 eV for 16 H/nm^2. However, it increases from 0.44 to 1.31 eV for a coverage of 16 to 20 H /nm^2, respectively In this case, there is a compromise between the concentration of protons and the activation energy. More protons at the surface are expected to reduce the reactivity of surface Ni atoms to break the C-O bond.

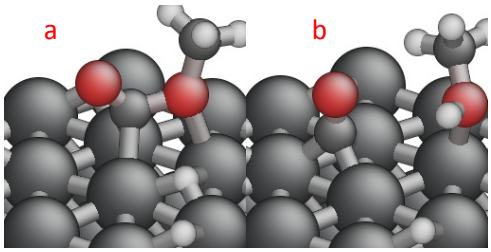

Fig. 3. Formation of methanol from CO_2CH_3; a) shows the adsorption of CH_3 to an adsorbate CO_2 molecule; and b) shows the formation of methanol and adsorbate CO.

3.1.2. Formaldehyde

Two reaction pathways are identified. First, CH_2 is introduced to a CO_2 adsorbate; see Fig. 4a. This adsorption will lead to the formation of CH_2O and CO: see Fig. 4b. In the second pathway, CH_2 is introduced to an adsorbed O atom, also leading to the formation and desorption of CH_2O.

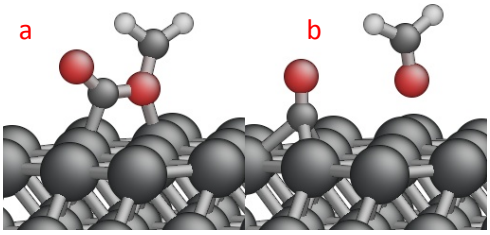

Fig. 4. Formation of formaldehyde; a) shows the adsorption of CH_2 to the adsorbate CO_2 molecule; and b) shows the formation of methanol and adsorbate CO.

3.1.3. Formic acid

The adsorption of three CO_2 molecules is shown in Fig. 5a. The proton coverage is 24 H/nm^2. Many protons are introduced to the carbon and oxygen of adsorbate CO_2 molecules. Ab initio MD simulation shows only the desorption of formic acid (HCOOH); see Fig. 5b. An activation energy of 0.12 eV is calculated by the NEB method. This activation energy is even reduced for higher proton coverage. This is the only observed reaction pathway for formic acid.

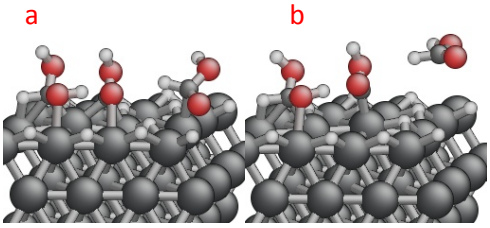

Fig. 5. Protonation of adsorbate CO_2 molecules to formic acid; a) shows the introduction of protons from the gas phase to adsorbate CO_2 molecules; and b) shows desorption of formic acid during ab initio MD simulation.

3.1.4. C1-C2 hydrocarbons

The protonation of C1 hydrocarbons for different H coverages at the surface is shown in Table 2 (reactions 1 to 6). The activation energy and reaction energetics of the protonation of CH_x (x = 0 to 3) are reported. The objective was to consider always the same proton for each coverage. The surface proton atoms are highly mobile and the position of the protons in each coverage is constantly changed. Protonation of CH_x is an exothermic reaction or it becomes exothermic for higher proton coverages. The activation energy is reduced with the increase of the proton coverage in all cases, as shown in Table 2.

Recombination of CH_x radicals at the surface will give rise to the formation of CH_y-CH_z (y and z = 1 to 3). Hydrocarbons like ethyne (CHCH) are less likely created and ethane (CH_3CH_3) will desorb from the surface. Desorption of ethane is an exothermic reaction. However,

desorption of CH_2CH_2 is an endothermic reaction. Hence, CH_2CH_2 will remain adsorbed to become more protonated.

The protonation of CH_3CH to CH_3CH_2 is also presented in Table 2 (reactions 7 to 9). As the proton coverage increases, the activation energy is reduced from 0.52 eV to 0.19 eV and protonation becomes more exothermic (ΔE = 0.03 eV to -1.03 eV). The same situation occurs for protonation of CH_3CH_2 to CH_3CH_3. The activation energy reduces for a higher proton coverage (Table 2: reactions 10 to 12) and the reactions become more exothermic.

Table 2. Protonation of C1-C2 hydrocarbons for different proton coverage.

Reaction	Coverage (H/nm^2)	E_a (eV)	ΔE
C1-hydrocarbon			
1. $C(s)+H(s)\rightarrow CH(s)$	12	0.27	-1.07
2. $CH(s)+H(s)\rightarrow CH_2(s)$	12	0.19	+0.14
3. $CH(s)+H(s)\rightarrow CH_2(s)$	16	0.08	-0.02
4. $CH_2(s)\rightarrow CH_3(s)$	8	0.19	-0.21
5. $CH_2(s)\rightarrow CH_3(s)$	16	0.05	-0.41
6. $CH_3(s)\rightarrow CH_4(g)$	12	0.46	-0.21
C2-hydrocarbon			
7. $CH_3CH(s)+H(s)\rightarrow CH_3CH_2(s)$	20	0.52	+0.03
8. $CH_3CH(s)+H(s)\rightarrow CH_3CH_2(s)$	24	0.21	-0.27
9. $CH_3CH(s)+H(s)\rightarrow CH_3CH_2(s)$	28	0.19	-1.03
10. $CH_3CH_2(s)+H(s)\rightarrow CH_3CH_3(g)$	12	0.78	-0.22
11. $CH_3CH_2(s)+H(s)\rightarrow CH_3CH_3(g)$	20	0.31	-0.35
12. $CH_3CH_2(s)+H(s)\rightarrow CH_3CH_3(g)$	24	0.26	-0.70
13. $CH_2CH_2(s)+H(s)\rightarrow CH_3CH_2(s)$	8	0.53	+0.29
14. $CH_2CH_2(s)+H(s)\rightarrow CH_3CH_2(s)$	20	0.45	+0.26
15. $CH_2CH_2(s)+H(s)\rightarrow CH_3CH_2(s)$	24	0.47	+0.02

Protonation of CH_2CH_2 to CH_3CH_2 is an endothermic reaction (Table 2: reactions 13 to 15). The activation energy for this reaction for different coverages is not significantly reduced, in contrast to the other protonation reactions in Table 2.

3.2. KMC results

More than 120 reactions from the atomic scale calculations (DFT) are translated into discrete events in order to describe the KMC simulation. The simulation box contains 6400 sites, of which 3200 sites are Ni sites in two layers as catalyst surface and 3200 sites are fcc and hcp sites at the top layer (empty sites); see Fig. 6. This leads to a surface area of 50 nm^2. The temperature is set to 400 K. Impingement rates are described by Maxwell-Boltzmann statistics.

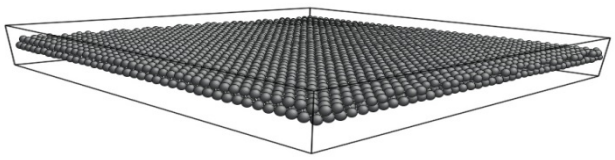

Fig. 6. KMC simulation box. Two layers of Ni are used to represent the catalyst surface.

Fig. 7 shows a snapshot of the surface after 10^{-7} s. During the course of the simulation, the number of each product species is counted, allowing to identify the dominant reaction pathways for various products, for different partial pressures of the radical species. Also, the competition between reaction pathways for various products can be analyzed. Knowledge about the chemical reaction pathways and the underlying chemical and physical reasons will allow us to design a plasma-catalytic process for specific added-value chemicals.

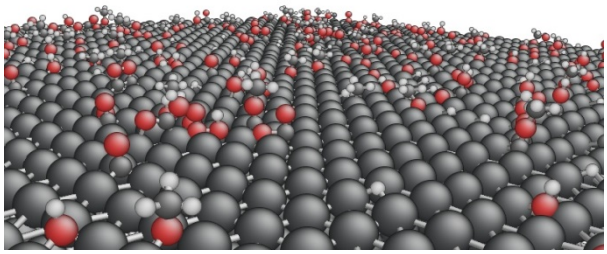

Fig. 7. Snapshot of the Ni surface after 10^{-7} s. The formation of fragment molecules can be observed (large grey = Ni, small grey = C, red = O, white = H).

4. Conclusion

We studied the fundamental chemistry of free radicals and molecules interacting with a Ni(111)-catalyst surface in the context of plasma catalysis. We identify the possible reaction pathways for the formation of added-value chemicals. All chemical reactions with underlying local chemistry are implemented as discrete events in an on-lattice KMC simulation. The combination of DFT and KMC methods offers a distinct method to identify the dominant reaction pathways.

5. Acknowledgements

This research was funded by the European Union Seventh Framework Programme (FP7-PEOPLE-2013-ITN) under Grant Agreement no. 606889 (RAPID - Reactive Atmospheric Plasma processIng – eDucation network). This research was also carried out in the framework of the network on Physical Chemistry of Plasma-Surface Interaction-Interuniversity Attraction Poles, phase VII (http://psi-iap7.ulb.ac.be/), and supported by the Belgian Science Policy Office (BELSPO).

6. References

[1] H.L. Chen, *et al. Environ. Sci. Technol.*, **43**, 2216 (2009)

[2] X. Tu and J.C. Whitehead. *Appl. Catal. B: Environ.*, **125**, 439 (2012)

[3] E.C. Neyts and A. Bogaerts. *J. Phys. D: Appl. Phys.*, **47,** 224010 (2014)

[4] W. Kohn, A.D Becke and R.G. Parr. *J. Phys. Chem.*, **100**, 12974 (1996)

[5] G. Kresse and J. Hafner. *Phys. Rev. B*, **47**, 558 (1993)
[6] G. Henkelman, B.P. Uberuaga and H. Jonsson. *J. Chem. Phys.*, **113**, 9901 (2013)
[7] A. Slepoy, A.P. Thompson and S.J. Plimpton. *J. Chem. Phys.*, **128**, 205101 (2008)
[8] M. Shirazi and S.D. Elliott. *J. Comput. Chem.*, **35**, 244 (2014)